THE ASTROPHYSICAL JOURNAL, 380:419–428, 1991 October 20

POLARIMETRIC IMAGING OF THE GALACTIC CENTER AT 12.4 MICRONS: THE DETAILED MAGNETIC FIELD STRUCTURE IN THE NORTHERN ARM AND EAST-WEST BAR

DAVID K. AITKEN,[1] DANIEL GEZARI,[2] CRAIG H. SMITH,[1] MARK MCCAUGHREAN,[2,3] AND PATRICK F. ROCHE[4]

Received 1991 February 4; accepted 1991 May 3

ABSTRACT

We present new closely sampled ($\sim 1''$) imaging polarimetry of the central 0.5 pc of the Galaxy at 12.4 μm with a 58 × 62 array camera system. The image shows a much more detailed view of the morphology of the intrinsically polarized emission (and the associated aligning magnetic field) in the ionized filaments of the Sgr A West complex than has been possible with earlier single beam studies.

The new results show that the magnetic field in the northern arm is continuous on 1″ scale and is a property of the filamentary structure rather than the compact peaks of infrared emission and that it continues in a southwesterly direction from IRS 1 for several arcseconds into the east-west bar. In the southern and western part of the east-west bar the intrinsic polarization becomes complex, with small-scale variations of polarization fraction and position angle, probably due to superposition of different field directions along the line of sight. There is no evidence of perturbation of the field structure by the energetic outflows from the IRS 16 complex, and it is concluded that IRS 16 does not lie in the plane of the northern arm, and that it cannot be at the center of the mass distribution of the Sgr A West system.

We consider that the magnetic field in Sgr A West is amplified due to shearing motions in the ionized material and that the direction of the field is that of the flow. The run of magnetic field directions in the inner rim of the northern arm and east west bar then indicate a flow pattern which shows striking symmetry about the position of Sgr A*. When earlier data from outside the image area are included, an elliptical flow pattern with focus close to Sgr A* is indicated.

Subject headings: galaxies: nuclei — galaxies: The Galaxy — interstellar: magnetic fields — polarization

1. INTRODUCTION

Following the discovery of infrared polarization from the Galactic center by Dyck, Capps, & Beichman (1974) further observations (Capps & Knacke 1976; Knacke & Capps 1977, hereafter KC; Lebofsky et al 1982) showed that there were marked spatial variations of the mid-infrared (8–13 μm) polarization over the central arcminutes of the region. In contrast, the polarization observed in the near-infrared is quite smooth and is attributed to interstellar polarization along the line of sight. Spectropolarimetric observations between 8–13 μm (Aitken et al 1986, Paper I) demonstrated that the mid-infrared polarization could convincingly be explained by polarized emission from warm aligned silicate grains within Sgr A West, overlaid by a uniform absorptive component of polarization due to aligned grains in the interstellar medium. It was further shown that grain alignment in Sgr A by streaming of grains through gas could be ruled out and that only a magnetic field directed along the northern arm provided a plausible alignment mechanism, revealing the presence of an organized magnetic field within the central parsec of the Galaxy.

The observational techniques of 8–13 μm polarimetry and the method of separating the intrinsic and interstellar components of polarization have been considered at length in Paper I; further results at mid- and far-infrared wavelengths (Werner et al 1988; Hildebrand 1989) and the implications of these results have been discussed by Aitken (1989, Paper II), and Hildebrand et al. (1990).

The association of mid- and far-infrared polarization with magnetic field direction is crucial to the interpretation followed in these previous works and in the present paper. In Papers I and II compelling arguments were presented for magnetic alignment of the grains in the ionized regions of Sgr A West. Additionally there are more general arguments which ensure that the orientation of grain alignment will (almost) always be controlled by the magnetic field even when some other mechanism actually produces the alignment, that is, produces an anisotropy in the grain spin distribution. These arguments are given in detail in § 4.1, together with some reemphasis of the discussion of Paper I.

For each of the sources observed within the northern arm (Papers I and II), vectors normal to the intrinsic polarization position angles trace out the line of the arm. For polarized emission this requires that the spin axes of the grains are aligned with the direction of the northern arm and implies a coherent magnetic field directed along the arm. In the east-west bar the intrinsic polarization is much smaller, and the position angles are not obviously correlated with the morphology; a magnetic field directed closer to the line of sight is a possible explanation.

The emissive component of polarization is particularly strong in the compact sources of the Northern Arm where its amplitude is nearly uniform in the range 7%–8% (Paper I); this represents a greater degree of alignment (by a factor of ~ 2) over any other polarized region studied to date. (The appropriate comparison for absorptive polarization is the specific polarization, or polarization per unit optical depth, p/τ; in the

[1] Department of Physics, University College, ADFA, University of New South Wales, Campbell, 2600, ACT, Australia.
[2] NASA/Goddard Space Flight Center, Infrared Astrophysics Branch, Code 685, Greenbelt, MD 20771.
[3] Postal address: Steward Observatory, Tucson, AZ 85721.
[4] Department of Astrophysics, Keble Road, Oxford University, Oxford OX1 3RH, England, UK

BN object in Orion, which has observed polarization of 12.7% at 10.2 μm, $p/\tau = 12.7/3.3 \simeq 4\%$.) As pointed out in Paper II this large polarization of uniform amplitude is independent of the small-scale structure in Sgr A and this suggests that there may be nearly complete alignment of the grains.

The presence of an organized magnetic field in the Galactic Center raises a number of questions. In particular, the continuous sampling and higher spatial resolution of the array camera polarimeter can be used to investigate the following points in more detail.

1. To what extent is the magnetic field a property of the discrete (and possibly embedded) sources rather than the diffuse material between them?
2. Is there a comparable field in the east-west bar, but directed more nearly along the line of sight?
3. How does the 7%–8% polarization at IRS 1 merge into the east-west bar where the polarization appears to be less than 2%?
4. Does the northern arm make an abrupt change of direction near IRS 1, as has sometimes been argued?

We present here the results of polarimetric imaging at 12.4 μm of a $\sim 14''$ field centered near Sgr A* with a spatial resolution $\simeq 0''.8$. This is the first mid infrared polarimetric image produced with an array camera. It demonstrates the viability of this method of studying detailed magnetic field morphology, free of the confusion of a scattering component to polarization which is prevalent at near-infrared wavelengths.

2. OBSERVATIONS

2.1. *Polarimetric Imaging at 12.4 Microns*

The 10 μm array camera (Gezari et al. 1991) developed at NASA/Goddard Space Flight Center is based on a 58 × 62 pixel Si:Ga photoconductor array manufactured by Hughes/Santa Barbara Research Center. The array and camera optics are cooled to 10 K with liquid helium. The optical system uses a single 3.0 inch focal length off-axis parabolic mirror as the only focusing element. The parabola reimages the focal plane on to the array with a demagnification of 2:1, resulting in an array plate scale on the UKIRT of $0''.21$ pixel^{-1} with a field of view of $11''.5 \times 12''.5$. A cold aperture stop at the image of the telescope secondary minimizes out-of-field background. In the present configuration an interference filter defined the spectral band pass of $\Delta\lambda/\lambda = 0.1$ centered at 12.4 μm. Spatial resolution was $1''.0 \pm 0''.1$ (chiefly seeing limited) measured from stellar images. Aberrations and distortion (pin cushion, etc) are negligible, and the array orientation error with respect to equatorial co-ordinates is less than $\frac{1}{2}$ degree. The array camera noise equivalent flux density (NEFD) at 12.4 μm on the UKIRT was 0.03 Jy pixel^{-1} minute$^{-1/2}$ (1 σ). A more detailed description of the instrument has been presented elsewhere (Gezari et al. 1988, 1991), and initial imaging results were presented at the Third Ames Detector Workshop (Gezari, Foltz, & Woods 1989).

These observations using the array camera were made on the United Kingdom Infrared Telescope (UKIRT) on 1989 July 25 and 26. For the purposes of imaging polarimetry a wire grid analyzer was mounted on the cold (liquid helium) surface in the array camera close to the image of the telescope secondary, and a rotatable half-wave plate was mounted on the telescope axis just above the dichroic feed. The f/36 chopping secondary was operated at 1 Hz and the array read out sequentially with an integration time per frame of 30 ms. A beam throw of $20''$ was used and images corresponding to source and sky were accumulated for 3 minutes each. This procedure was repeated with the wave plate rotated through 45° to sample the orthogonal polarization, and the sum and difference between these sets of data yielded images of the Stokes parameters I and Q. A repeat of this procedure with the wave plate initial position rotated through 22°.5 then gave an independent intensity image and Stokes parameter U.

During two nights of observation the cycle of operations was repeated 17 times on center positions within a few arcseconds from Sgr A* and a similar number on a nearby "blank sky" field. Much of the later stages of data reduction were done using the IRCAM software package available at the UKIRT. The final image size was greater than $14''$ but has been truncated to reduce some of the systematic errors of polarization due to incomplete coverage.

Calibration of the instrumental position angle was by reference to the known position angle in IRS 1 at this wavelength (Paper I) and also by referring other images of AFGL 2591 (obtained during the same run) to previous results from spectropolarimetry (Aitken et al 1988). We allowed for the wave-plate efficiency of 75% at 12.4 μm.

The derived polarization image is shown in Figure 1, in which the 12.4 μm polarization is denoted by the length and orientation of the vectors and overlaid on the intensity contours. In this display, only vectors from alternate pixels on alternate rows are shown (i.e., one out of four) after convolving with a Gaussian profile approximating the seeing conditions of $\simeq 1''$

2.2. *Comparison with Mid-Infrared Spectropolarimetry*

As this is the first application of imaging polarimetry in the thermal infrared it is important to make an assessment of the systematic errors which might be associated with the images. The individual integration times and intervals between wave-plate movements (a few minutes) are very much longer than those which have been employed in spectropolarimetry (typically a few seconds) in this wavelength region, and consequently systematic errors due to fluctuations and drifts in the telescope/sky background and seeing and tracking errors are likely to be worse.

Spurious polarizations may arise in a number of ways. The images from which Q and U are obtained by difference must be registered to high accuracy, to a small fraction of the scale size of image features. For parts of Sgr A West, and especially the edges of the emission features, lack of registration at the $0''.1$ level could give rise to spurious limb brightening of polarizations of up to 10% at the extreme edges of features. The individual images were registered by centroiding on the unresolved source IRS 3. A diagnostic of misregistration would be the appearance of orthogonal polarizations on either side of the feature; the polarization distribution in IRS 3 (Fig. 1) suggests that the image is relatively free of this effect. In a similar way, changes in seeing or telescope focus between images may account for the peripheral polarization in the image of this source (seen more clearly in Figs. 2 and 3), but such an effect should be much smaller for the diffuse and resolved emission which predominates in the rest of the image. Additionally, drifts in sky and telescope emission during an observation cycle to determine Q or U can cause a general "cast" or gradient of polarization over the image which would be most serious in regions of low intensity.

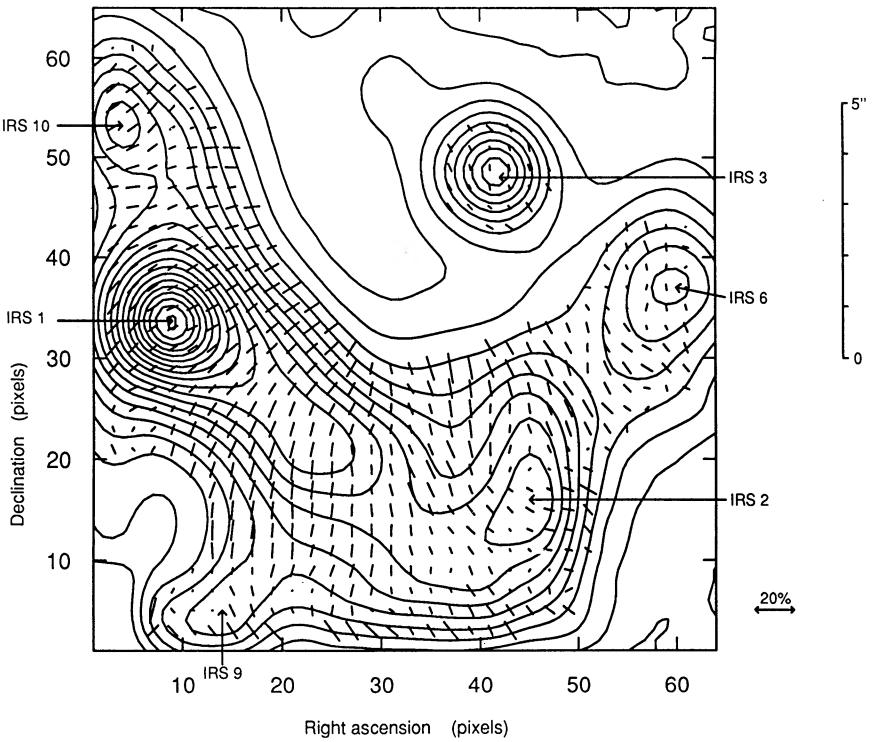

FIG. 1.—Observed 12.4 μm polarization vectors superposed on linearly spaced 12.4 μm brightness contours. Pixels are 0".21 on a side and axes are numbered in terms of pixel coordinates; north is to the top, and east to the left; these directions are within $\frac{1}{2}$ degree of the equatorial coordinate system. The scale is 0".21 pixel^{-1}.

To check the seriousness of these possible effects comparison has been made with spectropolarimetric observations of regions within Sgr A for which the polarization and position angle uncertainties are less than 0.25% and a few degrees, respectively; 12 of these positions are within the image field and their polarizations and position angles (Paper I, and hitherto unpublished data) are compared with the present work in Table 1. From such a comparison it appears that the image polarization is free of an overall systematic offset at the $\frac{1}{2}$% level but that there are random and area-dependent systematic errors amounting to $\sim \pm 1.2$%. Some of the discrepancies may be due to positional uncertainties in the spectropolarimetric data. In position angle the errors will naturally vary inversely with polarization; at 5% polarization the position angle error is approximately ± 8%. By way of example, the polarimetric images give an observed polarization near IRS 1 of $\simeq 5.2$% at 118°, whereas the spectropolarimetric results have consistently shown the polarization is 6.6 ± 0.5% at 131° $\pm$ few degrees here. Finally, below a brightness level ~ 10% of the peak the relative errors become too large to give trustworthy values for Q and U, and the polarization data has been suppressed from the images. Improvement in operating

TABLE 1

COMPARISON OF SPECTROPOLARIMETRIC AND CAMERA POLARIZATION PARAMETERS

	Offset[a]		Pixel Coordinates		Spectropolarimetry				Image				
Source	α	δ	α	δ	P	θ	Q	U	P	θ	Q	U	Notes[b]
IRS 1	...	...	9	33	6.6%	131°	−0.9%	−6.5%	5.2%	118°	−2.9%	−4.3%	1
IRS 2	7.5 W	4.0 S	45	15	2.1	38	0.5	2.0	3.2	63	−1.8	2.5	1
IRS 3	6.5 W	3.5 N	41	49	2.1	3	2.1	0.2	2.3	13	2.1	1.0	1
IRS 6	10.5 W	1.0 N	59	37	2.0	5	2.0	0.3	2.1	0	2.1	0.0	1
IRS 10	1.0 E	4.5 N	4	54	5.4	125	−1.85	−5.1	6.5	124	−2.4	−6.1	1
	5.0 W	4.0 S	32	11	2.0	18	1.6	1.2	4.4	3	4.3	0.5	1
	3.0 W	0.0 S	23	34	7.2	127	−2.0	−6.9	8.5	126	−2.7	−7.7	2
	3.0 W	3.0 S	23	20	8.6	162	7.0	−5.05	7.5	171	7.2	−2.2	2
	5.0 W	2.5 S	32	22	2.9	163	2.4	−1.6	4.0	10	3.7	1.4	2
	6.0 W	3.5 S	40	18	2.6	16	2.2	1.4	3.6	20	2.8	2.3	2
	9.0 W	0.5 S	53	30	3.7	26	2.3	2.9	4.9	28	2.7	4.1	3
	9.0 W	2.5 S	53	23	2.7	28	1.5	2.2	4.2	36	1.2	4.0	3

[a] Offset from IRS 1 in arcseconds.

[b] Comparison of 12.5 μm spectropolarimetic and 12.4 μm image observed polarization parameters. The spectropolarimetic values are evaluated from 12–13 μm using the data of Paper I (1), and observations later obtained at the UKIRT (2) and IRTF (3).

procedures, for which software development is currently under way, should substantially reduce most of these errors in future observing runs.

3. CORRECTION FOR THE INTERSTELLAR POLARIZATION

In general, there are two polarization processes contributing to the results shown in Figure 1; these are attributed to dichroic absorption by aligned silicate grains in the interstellar medium along the line of sight, and to polarized thermal emission from aligned grains within Sgr A (Paper I). IRS 3 is an example of a source which shows no emissive polarization and displays only the interstellar component (Paper I).

Since here we are only interested in the intrinsic polarization and its relation to the internal magnetic field in Sgr A, we need to devise a method for extracting the intrinsic polarization from the polarization images. In Paper I the absorptive component was unfolded from the data by treating the interstellar medium as an imperfect polarizer. The wavelength dependence of polarization adopted there was that of the BN object in Orion (Aitken, Smith, & Roche 1989) scaled to 5% at a position angle of 0°, the peak polarization and position angle of IRS 3 at 10 μm (this was done in preference to using the polarization of IRS 3 itself because the polarization spectrum of BN is of a much higher quality). BN is a molecular cloud source in which dust grains are not strictly similar to those in the interstellar medium, but within the limits of the observations, the form of the interstellar polarization observed against IRS 3 is essentially the same as that of BN. Using the BN polarization spectrum in this way yields an interstellar polarization to the Galactic center of 1.8% with position angle zero at 12.5 μm. Since publication of Paper I, further observations of IRS 3 (unpublished) are consistent with this estimate to $\pm 0.2\%$ and $\pm 3°$. With these values for the interstellar polarization the intrinsic polarization position angle of IRS 1 at 12.5 μm is just $7° \pm 0.8$ less than the observed value. Since the image polarization nowhere exceeds 10% it is sufficient to neglect cross terms involving interstellar and observed polarization in the transformation matrix and a simple subtraction of a polarization of 1.8% from the Stokes Q parameter will suffice to yield the intrinsic polarization.

Provided the same interstellar polarization applies over the whole image we can use this simple algorithm for each pixel to obtain the intrinsic polarization image. As long as the interstellar polarization is distributed over path lengths much longer than the lateral dimensions of the field it seems reasonable to consider that the interstellar extinction and polarization average to near constancy over the field. Interstellar extinction does appear to be sensibly constant over most of the region (e.g., Wade et al. 1987; Roche & Aitken 1985; Smith, Aitken, & Roche 1990), although near-infrared images due to Gatley et al. (1989) suggest larger extinction to the western edge of the Sgr A complex. This they attribute to the projection of the nearside rim of the molecular ring in front of Sgr A, and this might lead to increased extinction to IRS 6 and the nearby region. Indeed, the silicate absorption appears to be somewhat deeper to IRS 6 (Smith et al. 1990) than to the other 10 μm sources. While the interstellar polarization is related to the interstellar extinction, it depends also on other factors to do with ambient conditions along the line of sight. Again it seems reasonable to expect such variations to average out over such a relatively small field, and observations at 2.2 μm (Lebofsky et al. 1982; Kobayashi et al. 1980) indicate that this is the case. It is also possible to check the constancy of polarization through the "unfolding" procedure in Paper I. For all the strongly polarized sources in the northern arm and for IRS 2 this procedure (using the BN polarization spectrum scaled to 5% at 10 μm and P.A. 0°), results in an intrinsic polarization with the characteristic "tilde" spectral shape of polarized emission, and a position angle essentially independent of wavelength, and for IRS 3 negligible intrinsic polarization. (It is noticeable that IRS 3, which has deeper silicate absorption than the other sources, still accounts adequately for the interstellar polarization against the sources in the northern arm.) Most of the remaining sources are consistent with this interpretation, and we can thus be reasonably confident that the same interstellar polarization applies, except perhaps close to IRS 6.

The subtraction of a polarization of 1.8% from the Stokes parameter Q of each pixel of the image is shown in Figure 2, which then indicates the intrinsic polarization in the central region. For much of the discussion which follows, the grain spin alignment and the projected magnetic field direction are of greater interest, and these are obtained by a simple rotation of the intrinsic polarization vectors through $\pi/2$. The image obtained in this way is shown in Figure 3 in which the orientation of the axial vectors is that of the average projected magnetic field orientation, while their length is proportional to the intrinsic polarization and is a measure of the degree of grain alignment projected on the celestial sphere.

4. DISCUSSION

4.1. *Grain Alignment*

Two points developed in Paper I with respect to the role played by magnetic fields in grain alignment deserve reemphasis and amplification. First, while it was argued from considerations of the high degree of grain alignment required and from the morphology of the polarization in the northern arm that only magnetic alignment can provide a plausible mechanism, there is additionally a much more general argument that the polarization direction must (almost) always be determined by the ambient magnetic field. This is because spinning grains are self-magnetized by the Barnett effect (see, e.g., Landau & Lifshitz 1960, p. 144) and will precess about an ambient magnetic field. In itself this does not cause alignment, but because the precession period is much shorter than any of the likely alignment time scales, the orientation of any alignment, i.e., anisotropy in the distribution of grain spin axes, will then couple to the ambient magnetic field in almost any physically realistic astrophysical situation, irrespective of the direction of the aligning mechanism. For example, in the present situation of high density ($N_H \sim 10^5$ cm^{-3}) and temperature ($T \sim 10^4$ K) the disorienting time scale due to gas collisions is roughly a few years for grains of size 0.1 μm (e.g., Martin 1978), and for an alignment mechanism to be effective its time scale must be of this order. Due to the Barnett effect, paramagnetic grains of this size have magnetic moment $\mu \sim J$ ergs Gauss^{-1} (Dolginov & Mytraphanov 1976), where J is their angular momentum, and will precess about the ambient magnetic field with period $2\pi J/\mu B \sim 2\pi/B$. Even in an ambient magnetic field of as little as a few microgauss this period is only of order a few weeks, and unless an alignment mechanism operates on these time scales or less grain spin orientation will couple to the field direction. In such a situation, the degree of alignment will result from the cooperative action of the alignment mechanism and the orienting effect of the magnetic field and will be a maximum when these are parallel. That the polarization frac-

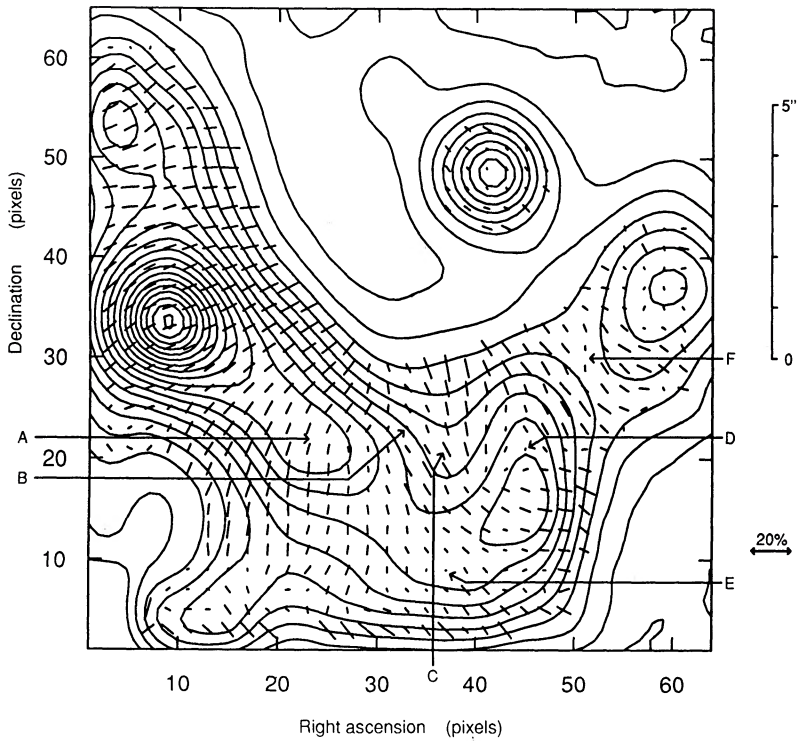

FIG. 2.—Emissive 12.4 μm polarization in Sgr A (after unfolding the interstellar polarization component—see text for details). Axes are as Fig. 1; the positions referred to in the text are indicated.

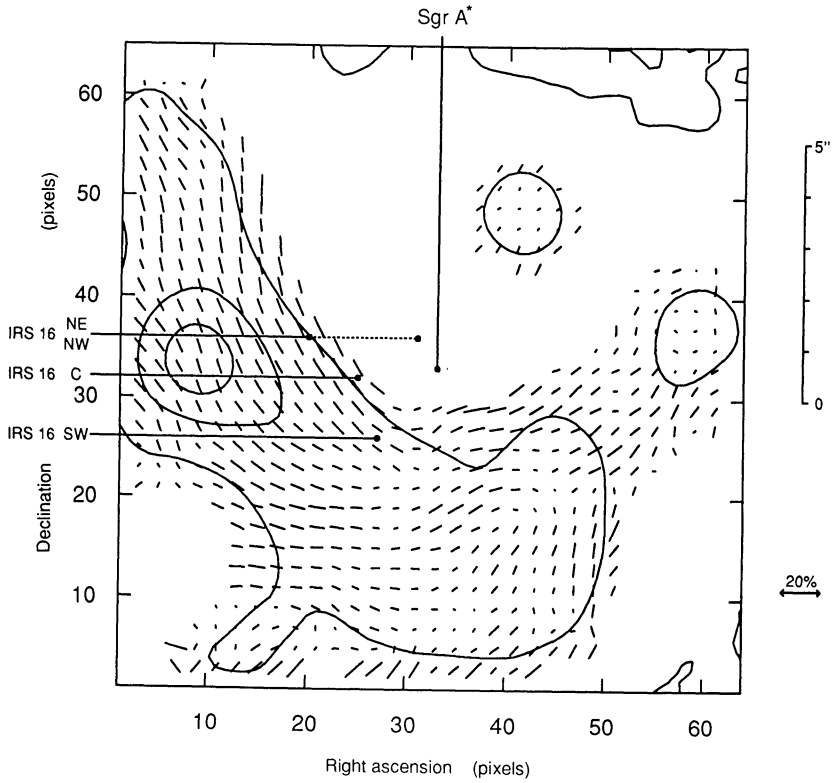

FIG. 3.—Grain alignment vectors in Sgr A. The vector positions here are orthogonal to those in Fig. 2 and the contour interval has been increased for clarity. The positions of Sgr A* and the components of IRS 16 are indicated.

tion in the northern arm is so nearly uniform is further evidence that alignment as well as orientation here is magnetic.

Second, even when the alignment is magnetic, as it is here, it seems that the classical Davis-Greenstein (DG) mechanism (Davis & Greenstein 1951) acting on paramagnetic grains in a magnetic field must operate in conjunction with one or more cooperative effects such as suprathermal rotation (Purcell 1979) and/or super paramagnetic (SPM) inclusions in grains (Jones & Spitzer 1967; Mathis 1986). The net result is that both the spin of the grains and their magnetic properties are uncertain, and a reliable estimate of the field strength from the DG mechanism is precluded. The value of $\simeq 10$ mG quoted in Paper I is derived from the classical DG mechanism operating on paramagnetic grains in equipartition with ions in an H II region and should therefore be regarded as no more than an order of magnitude estimate of the field strength. However, arguments of Chandrasekhar & Fermi (1953) based on the relationship between Alfvén velocities and the observed limits on turbulent motion place a lower limit of ~ 2 mG in the northern arm (Paper II).

Inspection of Figure 2 confirms the large, orderly, and nearly constant polarization fraction in the northern arm and shows that it extends to almost half-way between IRS 1 and IRS 2 with a smoothly changing position angle. This large polarization extends further up the arm, and, as shown in Paper I, at least to IRS 5, and the specific polarization is larger than so far observed elsewhere in the Galaxy. Further, the polarization shows no significant change in amplitude or direction between IRS 1 and the surrounding diffuse northern arm emission, in spite of changes of density and temperature in IRS 1 and IRS 10 with respect to the surrounding material. These temperature and density changes are indicated by the multicolor map of Smith, Aitken, & Roche (1990), which also shows that the radiation field in the diffuse regions is substantially harder than in and near IRS 1, and that silicate grains provide a greater fraction of the emission in IRS 1 than in the rest of the northern arm by a factor ~ 3. Knacke & Capps (1977) and Lebofsky et al. (1982) find substantial intrinsic polarization at 3.5 μm in IRS 1, 5, and 10, and in Paper I it is shown that after correction for the interstellar polarization the position angles of IRS 1 and 5 are consistent with those at 12.5 μm; here, apparently, very much hotter grains are also similarly aligned. The large and near constancy of mid-infrared polarization amplitude is then all the more remarkable since it implies uniform grain alignment through the whole of the material of the northern arm in spite of these different conditions.

The most straightforward inference from all this is that the grain alignment is almost or completely saturated; such an explanation would account for the non-dependence of grain alignment on physical conditions (but not for the apparent independence of polarization on grain chemistry, illustrated by the varying fraction of silicate emission with position). This view has been presented before (Paper II), but here the arguments are more cogent on account of the significantly greater spatial detail of the new polarization images. Saturated alignment implies that the magnetic field is correspondingly large and must be much larger in Sgr A than in other Galactic diffuse sources. The corollary to saturated alignment is that the polarization contains no information about the field strength, except by imposing a (poorly defined) lower limit on it, but that inferences may be made about its line of sight orientation as well as its projection on the celestial sphere.

4.2. *Intrinsic Polarization Distribution*

The general character of the intrinsic polarization in the northern arm is that it is of slowly varying amplitude, with a smoothly changing position angle which closely follows the normal to the direction of the arm. At IRS 1 the polarization amplitude given by the image is $\simeq 6.5\%$ with P.A. $\approx 111°$, (the more reliable spectropolarimetric value is 7.1% at 124°) and decreases to $\simeq 4.5\%$ at $\simeq 160°$ $\sim 3''$ southwest of IRS 1 (position A in Fig. 2). Continuing from here the polarization decreases rapidly and appears to go through a minimum $\simeq 2.5\%$ at a position 5″ west and 3″ south of IRS 1, just north of the ridge center line (position B). This region of small polarization is $\sim 2''$ in extent and oriented roughly southeast–northwest and is slightly to the east of a large change in the [Ne II] velocity (Serabyn et al. 1988). Following the ridge the polarization rises again reaching $\simeq 4\%$ with P.A. $\simeq 60°$ at IRS 2. Just north of the ridge center line (position C) the polarization rises much more rapidly reaching a maximum $\simeq 6.5\%$ with P.A. $\simeq 25°$, almost orthogonal to the position angle in IRS 1. Here there is a "valley" just north of the "saddle" between IRS 1 and 2, seen in previous 10 μm maps (e.g., Becklin et al. 1978), which coincides with the $\lambda = 2$ cm "minicavity" noted by Yusef-Zadeh, Morris, & Ekers (1989). IRS 2 is elongated in a north-south direction in the mid-infrared (Gezari 1989; Smith et al 1990) and double peaked in the radio continuum (Yusef-Zadeh et al. 1989). The southern end and eastern edge is a high-velocity region, the "-260 km s^{-1} cloud" of Lacy et al. (1980) and is polarized at the 4% level, but the northern part (the near-infrared source IRS 13, position D) appears to be a null polarization region, as does another region 2″ southeast (position E); at these positions the polarization is less than 0.5%. The region close to IRS 2 shows complex polarization structure. The "saddle" between IRS 2 and 6 (position F) is only weakly polarized ($\simeq 2.2\%$), but to either side along the ridge line the polarization is 5%–6% with position angle roughly normal to the ridge direction while IRS 6 itself appears to be essentially unpolarized. IRS 9 is quite close to the southern edge of the image in Figure 2, and because of this its polarization is uncertain; spectropolarimetry (Paper I) indicates $\sim 2\%$ polarization directed roughly normally to the ridge joining IRS 9 with the central ridge. Similarly at IRS 4, outside the image and to the east of Figure 2, the position angle is roughly normal to the line of the eastern arm (Paper I), and it seems that the emissive polarization from the eastern arm may be morphologically similar to that in the northern arm, that is a magnetic field directed along its length. Just to the northwest of IRS 9 (position G) there is a complex velocity region containing Lacy et al.'s (1980) "$+260$ km s^{-1} cloud," and this region shows little polarization. About 2″–3″ north of IRS 9 the polarization appears to merge into the southern edge of the northern arm system.

These details are consistent with the earlier spectropolarimetric results (Papers I and II), but now what is apparent is that the poorly defined and weak polarization in the east-west bar (when observed in six to eight positions with beam sizes in the 2″–4″ range) was the result of spatial averaging and incomplete sampling; with complete coverage at arcsecond resolution of the new images it becomes resolved into a complex of significantly polarized regions.

In the polarization images there is a small tendency for the polarization to increase along the northwestern rim of the northern arm. Such an effect may be an artifact of the observ-

ing procedure, as discussed in § 2.2 (however, the strong polarization is substantiated by spectropolarimetric observations 3″ west of IRS 1). Similarly some of the polarization features described above are not far from the 3 σ level of significance, and further observations with improved systematics are needed.

4.3. *Magnetic Field Distribution*

Much of what has been described above can be interpreted in terms of a projected magnetic field direction at right angles to the polarization vectors, and this is the interpretation on which Figure 3 is based. However, translation of polarization into magnetic field direction is not necessarily so straightforward, since we are dealing with a two-dimensional projection, and the intrinsic polarization is a superposition of polarizations within Sgr A along the line of sight. Where there is uniformity of polarization amplitude and position angle over dimensions similar to or greater than the lateral dimensions of features, as in the northern arm, it is reasonable to suppose that the polarization is sensibly constant along the line of sight. Along the northern arm there is strong added support for this simple interpretation since only a single velocity component with small gradient is involved (Serabyn & Lacy 1985). The normal to the polarization vector is then the magnetic field direction through the arm and earlier studies (Papers I and II) have shown that this reproduces the direction of the arm from $\sim$4″ southwest of IRS 1 to as far north as IRS 8. Figure 3 now demonstrates how uniform and continuous this field is over the extent of IRS 1 on much smaller scales, and that it follows the northern arm very smoothly into the central ridge; there is no evidence for a discontinuity in field direction at IRS 1 at the position of a "break" in the direction of the radio filament and where there appears to be a change in the velocity gradient (Serabyn et al 1988). If, as these authors suggest, these effects are due to a collision between converging filaments we would expect the magnetic field lines to be severely distorted.

The magnetic field distribution in the complex polarization regions of the east-west bar, from $\sim$4″ southwest of IRS 1, may not be as simple to unfold because of the likelihood of superposition of different polarizations, and here there are a number of possible interpretations. The grain alignment near a polarization minimum may still be uniform along the line of sight, in which case its projection on the celestial sphere would have to be small, implying a smaller degree of alignment (and possibly a smaller magnetic field) and/or oriented more nearly along the line of sight. Alternatively, the small lateral extent of the minimum regions suggests overlap between regions of different polarization, a view which is reinforced at position B by the proximity of almost orthogonally oriented polarizations on either side; the resultant of two such polarizations of nearly equal amplitude would be a polarization close to zero. These regions could still be part of the northern arm since here it appears to be closest to the line of sight, which is approximately tangent to the orbit. Due to the thickness of the northern arm, the line of sight will traverse regions in the orbit which have very different directions of motion; such a superposition could give rise to the reduced polarization.

It is possible that the minimum polarization region is the result of both projection and superposition. However, the increasing polarization to 5%–6% just to the west of this region indicates an increasing transverse component of velocity here, in a region where the radial velocity is still increasing (Serabyn et al. 1988). This would require that the perinucleus of the northern arm is much closer to IRS 2 than to IRS 1.

The polarization structure near position B could also be the result of the superposition of one or more neighboring but separate filaments in the vicinity of the closest approach to the dynamical center. The extension of the eastern arm would be a possible candidate for the additional flow, except that the low-velocity component of the [Ne II] line in the eastern arm does not continue into the east-west bar. Conceivably the excitation conditions in the putative extension of this arm are different so that Ne^+ is no longer the dominant state of neon, maybe due to a closer approach to the IRS 16 complex. In support of this it is noticeable that the [Ne II] emission is faint or absent along the western edge of the extended northern arm in the studies of Serabyn et al. (1988), and this is confirmed by low-resolution spectra which show a reduced [Ne II] equivalent width 3″ to the west of IRS 1 (unpublished).

If alignment is saturated throughout the region, the length of the polarization vector then gives information on the alignment component along the line of sight, and in positions B, D, and E a magnetic field directed close to the line of sight would be indicated. In particular, this implies that at position B the northern arm makes the smallest angle with the line of sight. The polarization $p \propto \cos^2 \theta$, where θ is the angle between the grain spin direction and the plane of the sky; if we take the polarization in the region of IRS 1, where the radial velocity is close to zero (Serabyn & Lacy 1985) as representing $p_{\max}$, where $\theta \simeq 0°$, then near position B, the region of minimum polarization along the northern arm,

$$\cos^2 \theta = p_{\min}/p_{\max} \sim 2.5/6.5 ,$$

and the magnetic field here would be $\sim$50° from the plane of the sky. This interpretation compares with Serabyn & Lacy's (1985) deduced rotation of $\sim$70° for the extended northern arm orbital plane from the plane of the sky which would correspond to a polarization of less than 1%. Such a discrepancy could well be attributed to superposition effects either in the northern arm along the line of sight or from unrelated structures.

The IRS 16 complex appears to be the origin of energetic outflows (Hall, Kleinmann, & Scoville 1982; Geballe et al. 1987) and has been suggested as the dominant source of luminosity in the central regions (Allen, Hyland, & Hillier 1990); however, it is not apparent in any of the 8–13 μm mid-infrared studies (see, e.g., Gezari 1989, Smith et al. 1990), or in the radio distributions (Yusef-Zadeh et al. 1989). Its position is indicated in Figure 3, and it is seen that although it is projected against a region of diffuse 10 μm emission, there is no sign of perturbation of either the polarization amplitude or direction. (However, as noted above, the [Ne II] equivalent width is small here.) As noted in Paper I, the ionized flows cannot penetrate the magnetic field of the arm but instead could distort the arm, and its magnetic field distribution, and this places constraints on the separation of IRS 16 from the arm. If the mass-loss rate in the IRS 16 flow is isotropic and $\sim 10^{-3}\ M_\odot\ \mathrm{yr}^{-1}$ (Gatley et al. 1984) with velocity $\approx$500 km s^{-1} (Allen, Hyland, & Hillier 1990), its pressure will equal the thermal pressure in the arm (taking the arm density as 10^5 cm^{-3} at 10^4 K) if IRS 16 is $\simeq$0.5 pc distant, giving a lower limit to the displacement, as long as the magnetic field $B \lesssim 2$ mG. If B exceeds this value, the magnetic pressure dominates and the distance constraint weakens; for a 10 mG magnetic field, the separation must exceed 0.1 pc, or 2″, and even then this should be resolved in the present image as a polarization disturbance of similar radius. The arm field could produce spectral and spatial asymmetries in the flow, however, and this may account for the red wing in the Brα

line profile of Allen et al. (1990), if IRS 16 lies on the far side of the arm. It must be concluded that if IRS 16 is the source of such an outflow, it does not lie in the plane of the northern arm and its extension, and that it cannot therefore be the mass center which controls this flow.

The embedded source which provides some local heating at IRS 1 (Smith et al. 1990), also does not disturb the polarization distribution; the inference here is that this source cannot be associated with strong dynamical activity. At IRS 2, on the other hand, the polarization distribution appears to be very disturbed; the two null positions with a magnetic field apparently directed between them is suggestive of a toroidal or a disk field with axis close to the plane of the sky. At IRS 10 there appears to be a local distortion of the field vectors which also coincides with a "kink" (*braiding*??) in the ionized filament. However, this latter region is close to the image boundary, and it is difficult to be sure that incomplete coverage may not be leading to a spurious result.

5. ROLE OF THE MAGNETIC FIELD

Far-infrared polarimetric observations of the 2 pc ring of molecular material around the Galactic center (Werner et al. 1988) indicate the presence of a magnetic field within the ring, and Zeeman observations (Schwarz & Lasenby 1989; Killeen, Lo, & Crutcher 1989) indicate that the field strength here is ~ 1 mG. Although the projected directions are well defined within the ionized filaments of Sgr A West, the strength of the magnetic field here is still uncertain on account of the uncertain magnetic properties of the grains and the possibility that grain alignment may be saturated. However, where comparisons with independent estimates of magnetic field are possible, the DG analysis overestimates the field by a factor between 3 and 10; use of such a correction factor here implies that magnetic field is greater than 1 mG. A field very much stronger than this limit would control the motion of the ionized material, and in such a case estimates of the mass distribution based on kinematics would be invalid. More recent Zeeman observation of a position within the northern arm (Roberts et al. 1991) yield an upper limit of 15 mG (3 σ) to the line-of-sight magnetic field. However, this only weakly constrains the magnetic field since at this position the radial velocity is small, the 12.5 μm polarization is large and the magnetic field must be largely transverse to the line of sight.

Indirect arguments, based on those of Chandrasekhar & Fermi (1953), indicate that the magnetic field in the northern arm is probably in the range of a few to a few tens milligrauss (Paper II). The energy density of such a field ranges from rough equality to a two order of magnitude increase over the thermal or turbulent energy of the ionized gas, but is not large enough to affect significantly the larger scale coherent motions. The direction of the magnetic field is then most likely the result of the shearing motions produced by tidal stretching, and thus, the magnetic field direction can indicate the orbital directions and in a more direct way than can be inferred from the morphology.

Serabyn et al. (1988) have drawn attention to the implicit assumption that the gas motion is along the direction of the filaments. In the region of the northern arm the run of magnetic field alignment seen in this and earlier work (Papers I and II) must be regarded as confirmation of this view. In regions of more confused morphology the magnetic field direction can help to clarify the flow complexity. For example, Figure 3 indicates that there is no evidence for a discontinuity in the flow near IRS 1 and that the apparent "break" at this position is more likely due to local density inhomogeneities and not to a discontinuity of flow direction.

It is of interest to correlate the polarization with the radial velocities of Lacy, Serabyn, Townes, and co-workers. We would expect a roughly inverse relation between polarization and radial velocity and indeed the largest values of polarization occur in the northern arm near IRS 1 where the radial velocity is small, while polarization tends to be small in regions of velocity complexity or where the velocity is large. An exception is the region close to IRS 2, where the polarization is still as much as $\simeq 4\%$ while the dominant velocity component is close to -260 km s^{-1}. If saturated alignment occurs here, a magnetic field inclined $\sim 50°$ to the line of sight is implied, and if this is the flow direction the velocity must then be ~ 400 km s^{-1}. There is a weak low-velocity component at IRS 2, and this may be associated with the polarization; to avoid problems with the expected dilution from the dominant high velocity component the latter would have to be associated with relatively weak infrared emission, and indeed this does seem to be the case (Gezari et al. 1989; Smith et al. 1990).

If grain alignment is saturated in Sgr A West, then there should be a strong correlation between polarization and radial velocity. Since $p \propto \cos^2 \theta$ and $V_r = V \sin \theta$ it is relevant to plot p against V_r^2; for a circular orbit we would expect a linear relationship of negative slope. Figure 4 shows a plot of radial velocities from Serabyn & Lacy (1985) and Serabyn et al. (1988) and polarizations taken from our image. These data are tabulated in Table 2. Only points along the northern arm and extended northern arm are presented and only where there is a single unambiguous [Ne II] velocity. There is a clear correlation ($r^2 = 0.34$, shown as a dotted line), which seems to indicate an increase in V_r^2 in excess of a linear relation at low values of p, and would be expected for a noncircular orbit. However, this effect depends mainly on the polarization data from west of the position of low polarization (position B, equivalently west of Sgr A*), which separately shows no corre-

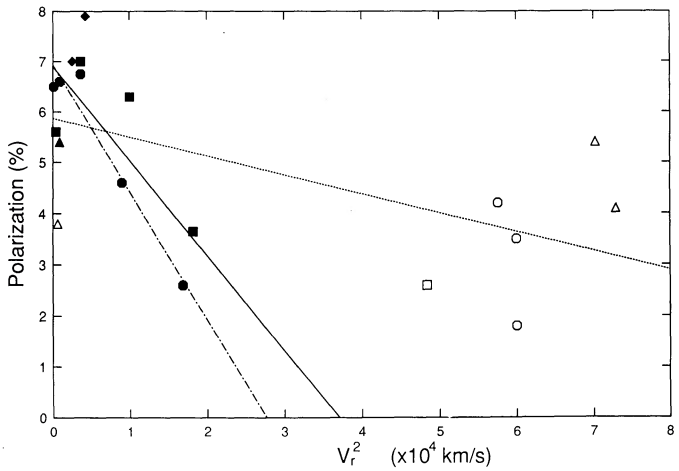

FIG. 4.—The polarization at 12.4 μm vs. (radial velocity)^2. Circles, squares, and triangles are from the central, east of center and west of center scans through the "central ridge" region (Serabyn et al. 1988, Figs. 2 and 4), respectively, while diamonds are from the northern arm observations of Serabyn & Lacy (1985, Fig. 2). Filled and open symbols refer to positions east and west of Sgr A*, respectively. The dotted correlation line is for all points ($r^2 = 0.34$), and the solid line is for points to the east of Sgr A* only ($r^2 = 0.57$). The dot-dashed correlation line refers to the central scans through the "central ridge" west of Sgr A* only (*filled circles*) and has $r^2 = 0.95$.

TABLE 2

COMPARISON OF IMAGE INTRINSIC POLARIZATION AND RADIAL VELOCITIES

Symbol[a]	Pixel Coordinates α	δ	P	θ	V_r (km s^{-1})	Reference
Filled circle	9	33	6.5%	111°	+10	1
	14	29	6.6	126	−30	1
	19	25	6.7	149	−60	1
	24	22	4.6	161	−95	1
	30	18	2.6	16	−130	1
Open circle	35	15	4.2	31	−240	1
	40	11	3.5	53	−245	1
	45	7	1.8	50	−245	1
Filled square	6	28	5.6	117	+20	1
	17	21	7.0	156	−60	1
	21	16	6.3	176	−100	1
	26	13	3.65	173	−135	1
Open square	37	6	2.6	44	−220	1
Filled triangle	7	42	5.4	105	+30	1
Open triangle	48	12	5.4	84	−265	1
	42	26	3.8	9	−25	1
	43	16	4.1	63	−270	1
Filled diamond	6	46	7.0	98	+50	2
	5	56	7.9	120	+65	2

REFERENCES.—(1) Serabyn et al. 1988; (2) Serabyn & Lacy, 1985.
[a] See Fig. 4.

lation, and the linear correlation is improved when this region is excluded; this is shown as a solid line ($r^2 = 0.57$). It is seen that there is still considerable scatter from the solid line, which may be expected if the region contains a spread of orbital parameters. If the comparison is restricted to a single "flow line" such as the velocity scan along the center line of the "central ridge" (Serabyn & Lacy 1985, Fig. 2) the correlation is now tight ($r^2 = 0.95$) and there is much less scatter (the filled circles and dot-dashed line in Fig. 4). This suggests that much of the scatter in the larger sample is the result of neighboring, but different, orbital parameters and the data give support to the notion of saturated grain alignment. To the extent that this section of the orbit can be approximated by a circle, the intercept on the V_r^2 axis corresponds to a circular speed of 165 km s^{-1}.

Serabyn et al. (1988) consider that the northern arm continues through the central region and that it extends to and includes the −260 km s^{-1} region at IRS 2. However, the coherent magnetic field structure of the northern arm does not continue further to the west than position B, and beyond here the polarization shows complex structure (outlined in §§ 4.2 and 4.3) and considerable disturbance around IRS 2. The poor correlation of p with V_r west of position B, and the clear lack of continuity with the northern arm data (Fig. 4) indicate that IRS 2 is an unrelated entity, seen perhaps in projection against the rest of the east-west bar. The velocity profiles of Serabyn et al. (1988) appear to be consistent with this view.

The region ∼2″ north of IRS 2 is not inconsistent in polarimetry or velocity with being an extension of the northern arm (pixel coordinates 42 and 16), and we have already remarked that the magnetic field distribution shows evidence for symmetry about Sgr A* (and not the IRS 16 complex). When some positions outside the image (IRS 5, IRS 8, and an intermediate position [from Papers I and II]) are included, an elliptical path through these and the western and northern rim of the northern arm and east-west bar has local direction close to the field directions and suggests continuity of flow along this path, which extends as far as a few arcseconds north of IRS 2. The major axis of the ellipse is approximately north-south and passes within 1″ of Sgr A* with an apparent focus ∼1″ south of it; after allowing for projection effects of an orbital plane tilted at 45° to the line of sight (see below) the focus of the Keplerian ellipse falls very close to Sgr A*. Unfortunately the velocity information relating to this part of the image (the northeastern edge of the "central ridge" of Serabyn et al. 1988, Figs 2 and 4) is very sparse as the [Ne II] line has weak equivalent width or is absent here.

It is difficult to reconcile the polarimetry data with an orbital plane inclined as much as 70° from the plane of the sky since in some regions (particularly one a few arcseconds south of Sgr A*) back projection implies that normally viewed polarizations would exceed 20%. While such large emissive polarizations cannot be excluded in principle, they are at least implausible and certainly would be unique. Thus it is very unlikely that the alignment in these parts of the image could be associated with a plane inclined by more than 45°.

Finally, we note that the model of Wardle & Königl (1990), which fits the observations of Hildebrand et al. (1990), leads to a magnetic field in the 2 pc molecular ring with both radial and circumferential components. It seems plausible that the northern arm is an infalling streamer from this ring with possible origin near IRS 8, and that the arm field has been amplified and oriented by tidal shearing.

6. CONCLUSIONS

The high spatial resolution imaging polarimetry reported here provides answers to some of the questions posed in § 1.

1. It is clear that the magnetic field is a property of the diffuse material of the large-scale structures in Sgr A (the northern arm and east west bar) rather than the embedded sources. The magnetic field is independent of the changes of density and temperature in the compact source environments.
2. The magnetic field direction in much of the east-west bar is complex, and its polarization is probably the result of superposition of differently oriented filaments.
3. The abrupt decrease of polarization southwest of IRS 1 observed previously (Papers I and II) is confirmed and shown to reverse sign. This is due either to a rapid change of magnetic field direction close to the dynamical center, or to the superposition of nearly orthogonal fields.
4. The field direction changes smoothly across IRS 1 and there appears to be no discontinuity of motion here, such as have been inferred from radio studies.

The region close to IRS 2 (the −260 km s^{-1} region) shows complex variations of polarization which may be due to an embedded source. It is not likely that the polarization observed here can arise from grain alignment in an extension of the northern arm as suggested by Serabyn et al. (1988).

From the lack of disturbance to the polarization vectors in that region of the northern arm which is in the same line of sight as the IRS 16 outflow complex, it can be inferred that IRS 16 must be significantly separated from the northern arm along the line of sight. From this we conclude that this complex does not lie in the plane of the northern arm and its extension and that it cannot be the dynamical mass center which controls this feature.

We interpret the magnetic field directions in Sgr A West as due to shearing in the ionized gas and that they indicate relative motion of the material. The symmetry of magnetic field directions around Sgr A* and the increasing curvature of these directions in its close vicinity then point to Sgr A* as the significant concentration of mass. However, to avoid the implications of excessive polarizations implied by large inclinations it seems that the plane of the northern arm can be tilted by no more than $\simeq 45°$ from the plane of the sky.

These are the first polarimetric images obtained in the thermal infrared; we expect that with improved operating procedures, systematic and other errors would be greatly reduced. In future studies, the flow pattern of the region, coupled with radial velocity information, could be used to investigate the form of the mass distribution within the central few tenths of parsec of the Galaxy.

We are grateful for the assistance of the staff of the UKIRT. Thanks also due to PATT for the award of observing time, and to the Australian Research Council, the SERC and NASA for contributions to funding. The Goddard Infrared Array Camera program is supported by NASA/OSSA RTOP No. 685-188-44. Larry Woods and Walter Folz at NASA/Goddard have made important contributions to the success of this programme. We also acknowledge useful discussions with Gene Serabyn. While at Goddard M. McCaughrean was supported by the National Research Council as an NRC Resident Research Associate.

REFERENCES

Aitken, D. K. 1989, IAU Symp. 136, The Center of the Galaxy, ed. M. Morris (Dordrecht: Reidel), 457 (Paper II)
Aitken, D. K., Roche, P. F., Bailey, J. A., Briggs, G. P., Hough, J. H., & Thomas, J. A. 1986, MNRAS, 218, 363 (Paper I)
Aitken, D. K., Roche, P. F., Smith, C. H., James, S. D., & Hough, J. H. 1988, MNRAS, 230, 629
Aitken, D. K., Smith, C. H., & Roche, P. F. 1989, MNRAS, 236, 919
Allen, D. A., Hyland, A. R., & Hillier, D. J. 1990, MNRAS, 244, 706
Becklin, E. E., Mathews, K., Neugebauer, G., & Willner, S. P. 1982, ApJ, 219, 121
Capps, R. W., & Knacke, R. F. 1976, ApJ, 270, 76
Chandrasekhar, S., & Fermi, E. 1953, ApJ, 118, 113
Davis, L., & Greenstein, J. L. 1951, ApJ, 114, 206
Dolginov, A. Z., & Mytraphanov, I. G. 1976, Ap. Space Sci., 43, 291
Dyck, H. M., Capps, R. W., & Beichman, C. A. 1974, ApJ, 188, L103
Gatley, I., Jones, T. J., Hyland, A. R., Beattie, D. H., & Lee, T. J. 1984, MNRAS, 210, 565
Gatley, I., Joyce, R., Fowler, A., DePoy, D., & Probst, R. 1989, IAU Symp. 136, The Center of the Galaxy, ed. M. Morris (Dordrecht: Reidel), 361
Geballe, T. R., Wade, R., Krisciunas, K., Gatley, I., & Bird, M. C. 1987, ApJ, 320, 562
Gezari, D. Y. 1989, IAU Symp. 136, The Center of the Galaxy, ed. M. Morris (Dordrecht: Reidel), 465
Gezari, D. Y., Folz, W. C., & Woods, L. A. 1989, Proc. 3d Infrared Detector Technology Workshop, ed. C. McCreight (NASA TM 102209), 267
Gezari, D. Y., Folz, W. C., Woods, L. A., & Wooldridge, J. 1988, Cryogenic Optical Systems and Instruments III (Proc. SPIE., 973), 287
Gezari, D. Y., Folz, W. C., Woods, L. A., Wooldridge, J., & Varosi, F. 1991, Opt. Eng., submitted
Hall, D. N., Kleinmann, S. G., & Scoville, N. Z. 1982, ApJ, 262, L53
Hildebrand, R. H. 1989, IAU Symp. 135, Interstellar Dust, ed. L. J. Allamandola & A. G. G. M. Tielens (Dordrecht: Reidel), 275
Hildebrand, R. H., Gonatas, D. P., Platt, S. R., Wu, X. D., Davidson, J. A., Werner, M. W., Novak, G., & Morris, M. 1990, ApJ, 263, 114
Jones, R. V., & Spitzer, L. 1967, ApJ, 147, 943
Killeen, N. E. B., Lo, K. Y., & Crutcher, R. 1989, IAU Symp. 140, Galactic and Intergalactic Magnetic Fields, ed. R. Beck, P. Kronberg, & R. Wielebinski (Dordrecht: Kluwer), 382
Knacke, R. F., & Capps, R. W. 1977, ApJ, 216, 271 (KC)
Kobayashi, Y., Kawara, K., Kosaza, T., Sato, S., & Okuda, H. 1980, PASJ, 32, 291
Lacy, J. H., Townes, C. H., Geballe, T. R., & Hollenbach, D. J. 1980, ApJ, 241, 132
Lacy, J. H., & Serabyn, E. 1985, ApJ, 293, 445
Landau, L. D., & Lifshitz, E. M. 1960, Electrodynamics of Continuous Media (Reading, MA: Addison-Wesley), 144
Lebofsky, M. J., Rieke, G. H., Deshpande, M. R., & Kemp, J. C. 1982, ApJ, 236, 672
Martin, P. G. 1978, Cosmic Dust (Oxford: Clarendon), 22
Mathis, J. S. 1986, ApJ, 308, 281
Purcell, E. M. 1979, ApJ, 231, 404
Roberts, D. A., Goss, W. M., van Gorkom, J. H., & Leahy, J. P. 1991, ApJ, 366, L15
Roche, P. F., & Aitken, D. K. 1985, MNRAS, 215, 425
Schwarz, U. L., & Lasenby, J. 1989, IAU Symp. 140, Galactic and Intergalactic Magnetic Fields, ed. R. Beck, P. Kronberg, & R. Wielebinski (Dordrecht: Kluwer), 383
Serabyn, E., & Lacy, J. H. 1985, ApJ, 293, 445
Serabyn, E., Lacy, J. H., Townes, C. H., & Bharat, R. 1988, ApJ, 326, 171
Smith, C. H., Aitken, D. K., & Roche, P. F. 1990, MNRAS, 246, 1
Wade, R., Geballe, T. R., Krisciunas, K., Gatley, I., & Bird, M. C. 1987, ApJ, 320, 570
Wardle, M., & Königl, A. 1990, ApJ, 362, 120
Werner, M. W., Davidson, J. A., Morris, M. R., Novak, G., Platt, S. R., & Hildebrand, R. H. 1988, ApJ, 333, 729
Yusef-Zadeh, F., Morris, M., & Ekers, R. 1989, IAU Symp. 136, The Center of the Galaxy, ed. M. Morris (Dordrecht: Kluwer), 443.